Physica Medica 64 (2019) 54–68

Contents lists available at ScienceDirect

Physica Medica

journal homepage: www.elsevier.com/locate/ejmp

Original paper

Optimization of Phase Space files from clinical linear accelerators

Juliana Cristina Martins[a,*,1], Rangoli Saxena[a,1,2], Sebastian Neppl[b], Abdulaziz Alhazmi[a], Michael Reiner[b], Stella Veloza[a,3], Claus Belka[b,c], Katia Parodi[a]

[a] Department of Medical Physics, Faculty of Physics, Ludwig-Maximilians-Universität München, Am Coulombwall 1, 85748 Garching b. München, Germany
[b] Department of Radiation Oncology, University Hospital, LMU Munich, Marchioninistraße15, 81377 Munich, Germany
[c] German Cancer Consortium (DKTK), Pettenkoferstraße 8a, 80336 Munich, Germany

ARTICLE INFO

Keywords:
Monte Carlo
Phase Space
Medical Linear Accelerator (linac)

ABSTRACT

This work proposes a methodology to produce an optimized phase-space (PhSp) for the Elekta Synergy linac by tuning the energy and direction of particles inside the 6-MV Elekta Precise PhSp, provided by the International Atomic Energy Agency (IAEA), for Monte Carlo (MC) simulations. First, the energies of the particles emerging from the original PhSp were increased by different factors, producing new PhSps. Percentage depth dose (PDD) profiles were simulated and compared to measured data from a Synergy linac for 6-MV photon beam. This process was repeated until a minimum difference was reached. Particles' directions were then manipulated following identified correlations to lateral profiles, resulting in two distinct perturbation factors based on inline and crossline profiles. Both factors were merged into one single optimal factor. For energy optimization, an increase of 0.32 MeV applied to all particles inside the original PhSp, but to 0.511 MeV annihilation photons, provided the best results. The direction optimization factor was the combination of the individual factors for inline (0.605%) and crossline (0.051%). The agreement between measured and simulated profiles, when using the optimized PhSp, improved considerably in comparison to simulations performed with the original IAEA PhSp. For all fields and depths analyzed, the discrepancies for PDD, inline and crossline profiles dropped from 11.2%, 15.7% and 27.5% to under 1.4%, 4.7% and 13.2%, respectively. The optimized PhSp should not replace the full linac modelling, however it offers an alternative for MC dose calculations when neither geometric details nor validated IAEA PhSp are available to the user.

1. Introduction

Monte Carlo (MC) techniques are considered the most accurate tool in determining the dose deposited to a medium by ionizing radiation, offering powerful numerical solutions to problems with high complexity. They have been proven mathematically to be more advantageous than analytic algorithms for problems with high number of parameters [1], such as the dose received by a patient due to radiotherapy treatments, especially at regions with high heterogeneity [2–4]. Thus, their applicability in radiation therapy has greatly increased in the last decades [5], being used for equipment design and optimization, radiation detector response and treatment planning [6].

However, the quality of the output depends strongly on the accuracy of the model. A precise characterization of the linear accelerator (linac) geometry is required, as well as the correct modelling of the initial electron beam incident on the target [7]. Discrepancies in the equipment modeling will result in systematic errors to patient dose calculation [8]. Detailed geometric information of the linac's components are often a commercial secret and hardly disclosed by the vendors, making the faithful modelling of the equipment a difficult task. One alternative is to replace the static part of the linac head by validated Phase Space (PhSp) files, which contain relevant information of particles crossing a reference surface (PhSp plane) positioned downstream the treatment head in the beam traveling direction. Several papers have investigated

* Corresponding author.
E-mail addresses: Juliana.Martins@physik.uni-muenchen.de (J.C. Martins), RSaxena@neuro.mpg.de (R. Saxena), Sebastian.Neppl@med.uni-muenchen.de (S. Neppl), Abdulaziz.Alhazmi@physik.uni-muenchen.de (A. Alhazmi), Michael.Reiner@med.uni-muenchen.de (M. Reiner), Lsvelozas@unal.edu.co (S. Veloza), Claus.Belka@med.uni-muenchen.de (C. Belka), Katia.Parodi@physik.uni-muenchen.de (K. Parodi).

[1] Both authors contributed equally to the work and are thus listed in alphabetic order.
[2] Present Address: Max Planck Institute of Neurobiology, Am Klopferspitz 18, 82152 Martinsried, Germany.
[3] Present Address: Departamento de Fisica, Universidad Nacional de Colombia, Carrera 30 No. 45 03, 111321 Bogota, Colombia.

https://doi.org/10.1016/j.ejmp.2019.06.007
Received 7 December 2018; Received in revised form 5 June 2019; Accepted 15 June 2019
Available online 24 June 2019

the use of PhSp files for linac MC modeling [6,9,10]. The use of PhSp also improves the simulation time, as the radiation transport through the static parts of the linac does not need to be repeatedly simulated [11], although full-linac simulations can potentially be as time-efficient, provided proper variance reduction techniques are employed [12]. The International Atomic Energy Agency (IAEA) provides a database of fully validated PhSp files, available for general use [13], which can be implemented with different general purposes MC codes like EGSnrc [14], PENELOPE [15] and Geant4 [11]. Currently, the IAEA database offers validated PhSp for only a limited number of linac models.

In a previous study we attempted to model a 6-MV photon beam produced by an Elekta Synergy® linac equipped with the Elekta Agility™ collimator. Due to unavailability of geometric information of the linac head and of a correspondent validated PhSp, the IAEA PhSp for an Elekta Precise® was used as a surrogate for the static part of the equipment. Discrepancies as high as 11.2% and 26.3% were observed for Percentage Depth Dose (PDD) and lateral profiles, respectively, when compared to measurements. These discrepancies can be attributed to differences in linacs' geometries and initial electron focal spots. The electron source of the Elekta Precise model used to generate the correspondent IAEA PhSp was defined as a circular-shaped electron beam [16], a method also adopted by other authors [17,18]. For the Elekta Synergy, better results have been reported when an elliptical electron source is used [7,19]. Measurements performed with the Synergy linac used in this study have also indicated an elliptical source. Moreover, the output of a linac simulation is very sensitive to the geometry of the head components, such as the primary collimator and flattening filter [20]. Therefore, without detailed information or a proper validated PhSp, this approach failed to simulate the Synergy linac correctly.

The present work proposes a methodology to manipulate the information stored by a validated IAEA PhSp, in order to produce an optimized PhSp that can yield improved results for modeling a different equipment, offering an alternative when neither the geometry nor the IAEA PhSp of the linac model under interest are available. In this study, the Elekta Precise IAEA PhSp was used as the starting point to produce a suitable PhSp for the Elekta Synergy linac, for the 6-MV photon beam. First, the energy of the particles was perturbed until a minimum difference between simulated PDDs and respective measurements was achieved. The effect of the energy optimization on the lateral profiles (inline and crossline directions) was also evaluated. Next, the particles' travelling directions were perturbed randomly, resulting in perturbations to the total angular distribution, and lateral profiles were simulated iteratively, to identify correlations of this information with the simulated profiles. Subsequent perturbations were performed respecting identified correlations, following the tendency of decreasing cost values (quantified discrepancies between simulated and measured data). Optimal perturbation factors were identified for both energy and directions and used to produce the new PhSp. The optimized PhSp was validated against dosimetric measurements for different fields at two different depths in water.

2. Materials and methods

The IAEA PhSps are binary files containing information regarding particles' position, energy and direction, along with supplementary parameters that are not considered in this study. In addition, the information is stored in an unknown sequence, thus the extraction of selected information becomes unfeasible. To overcome this issue a new PhSp, hereon referred to as LMU PhSp, was positioned 27.9 mm beneath the IAEA PhSp and recorded the relevant parameters from particles emerging from the former. This study focuses on the optimization of the energy and direction of the particles, as these parameters can be directly connected to properties of the electron source and the focal spot.

The optimization was an iterative process in which the energy or direction of the particles in the LMU PhSp was perturbed, and for each perturbation a new PhSp was generated. The perturbed PhSp was used to simulate PDDs and lateral profiles (inline and crossline directions) in a virtual water phantom. Simulated profiles were compared to measured data acquired under the same conditions in water. These steps were repeated until an optimal perturbation for energy and directions was found, i.e. until a good agreement between simulations and measurements was obtained. This agreement was quantified in terms of cost values (described in Section 2.2). For energy optimization, the cost value between measured and simulated PDD was used as a benchmark, as the PDD is strongly dependent on the energy of the photon beam [21]. The angular distribution of the particles is described in terms of their direction cosines, and is connected to the spatial distribution of the focal spot, which has a strong effect on the lateral profiles [7,22], particularly at the penumbra region. In this study, the penumbra region is taken as the region between the 80% and 20% dose levels. Therefore the cost values for the lateral profiles were chosen as a reference for direction optimization, focusing on the penumbra. To improve this iterative process, the PhSps were cropped into smaller circular sections, depending on the field size and on the profile to be simulated. More details are given in Section 2.3.

2.1. Measurements and simulations

All measurements were performed in an Elekta Synergy® linac equipped with an Elekta Agility™Multi Leaf collimator (MLC) (Elekta Oncology Systems, Crawley, UK), with a fixed collimator angle (0°), for a 6-MV photon beam. PDD and lateral profiles for 2×2, 5×5, 10×10 and $20 \times 20\,\text{cm}^2$ fields were measured in a water phantom (Blue Phantom, IBA Dosimetry, Schwarzenbruck, Germany) with a microDiamond detector (P60019, PTW, Freiburg, Germany), at source-to-surface distance of 900 mm. The PDD profiles were measured from the surface of the water to 300 mm depth, with 1-mm steps in the build-up region. The step size increased to 2 mm up to the 50th measuring point and further increased to 4 mm for the rest of the measurement. Lateral profiles were measured at 15 mm and 100 mm depths in water, with 1-mm steps in the penumbra region and 4 mm elsewhere. Profiles at 15 mm depth were used for optimization, while validation was performed for both depths.

PDD and lateral profiles were simulated under the same conditions in a virtual water phantom, using an in–house developed MC model of the Agility MLC. The perturbed PhSps were used as surrogates for the static part of the linac head. Particle recycling ranged from 14 to 24 times, depending on the field size and on the PhSp used: for cropped PhSp (Section 2.3) 24 times recycling was used due to the reduced number of available particles; for simulations performed with full PhSp, particles were recycled 14 and 19 times for smaller and larger fields, respectively.

For both PDD and lateral profiles, the dose was recorded using the command-based scoring feature from Geant4, hereon referred to as scoring meshes. Column-like scoring meshes were used for PDD simulations, with 1-mm resolution in the central axis direction, to account for the doses at different depths in water. For lateral profiles, two-dimensional (2D) scoring meshes were used with 1-mm resolution in the inline and crossline directions. The total size of the 2D mesh is determined such that it scores the entire penumbra region, and is therefore dependent on the field size. The simulation uncertainties were calculated using the batch-approach [23] considering voxels which scored at least 10% of the maximum dose, as in low dose areas (e.g. profile tails) fewer interactions take place and a non-representative increase in the uncertainty is observed. For all simulations performed, the average uncertainty was 2%, with a maximum value of 3%. All simulations were performed using Geant4 v.10.01.p01.

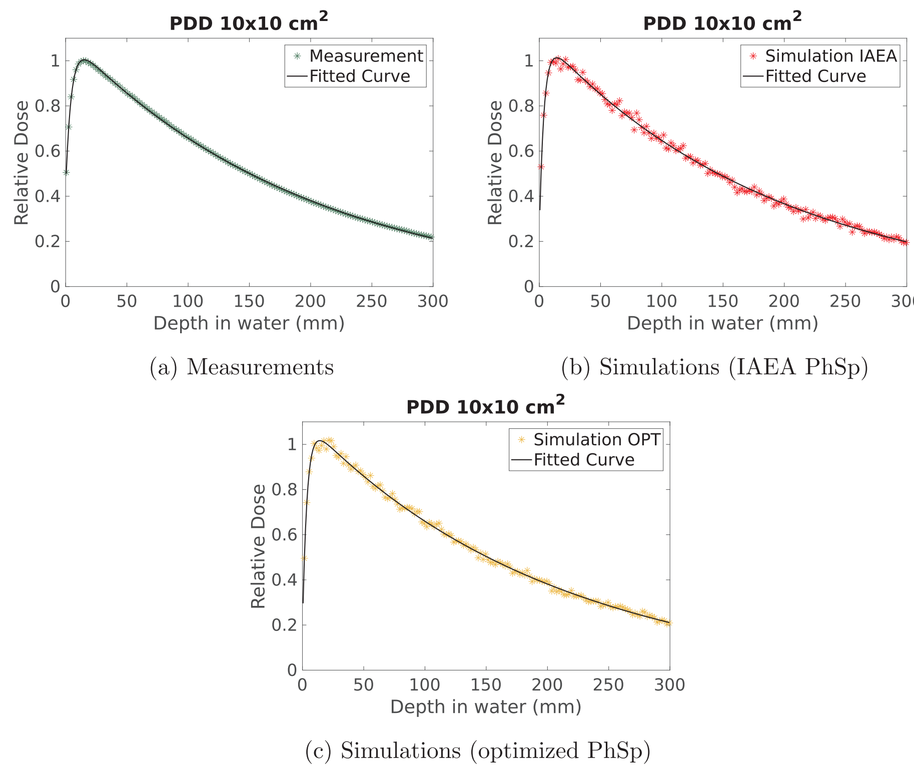

Fig. 1. PDD profiles fitted curves for the $10 \times 10\,cm^2$ field: for (a) Measurements, (b) Simulations performed with the original IAEA PhSp and (c) Simulations performed with optimized PhSp. For all three data sets, the adjusted R^2 values are higher than 0.996; RMSEs are smaller than 0.015.

2.2. Cost values

To account for the different sampling spacing, the data for both measured and simulated profiles were fitted to continuous functions. The difference between the fitted curves can be quantified and reflects the disagreement between the data. For the PDD, a double exponential (Eq. (1)) was used as a fitting function. Here, $D(d)$ is the dose at depth d and a_1, a_2, b_1, b_2 and c are the fitting parameters. Both curves were fitted to the same domain ($d = [0, 300]$ mm). For visualization, Fig. 1 shows the fitted PDD curves for the $10 \times 10\,cm^2$ field for measured and simulated data. For all data sets and all fields analyzed, the adjusted R^2 values are greater than 0.996 and the Root Mean Square Errors (RMSEs) are lower than 0.016.

$$D(d) = a_1 e^{-b_1 d} - a_2 e^{-b_2 d} + cd \tag{1}$$

$$\chi^2 = \frac{1}{n}\sum_{i=1}^{n} \left(D_i^{(m)} - D_i^{(s)}\right)^2 \tag{2}$$

The discrepancy, referred to as cost value, is given by a χ^2 function (Eq. (2)). $D_i^{(m)}$ and $D_i^{(s)}$ are the doses at point i, for the fitted curves of the measured and simulated PDD, respectively. n is the total number of points used in the calculation of the cost, which ranges from 0 to 300, to account for the region considered for PDD simulations and measurements.

The lateral profiles were fitted using a sigmoid function (Eq. (3)), where the parameters k and x_0 represent the slope and the position of the center of the sigmoid, respectively, and $D(x)$ is the dose at a position x. Fig. 2 shows the fitted crossline profiles, at 15 mm depth in water, for the $10 \times 10\,cm^2$ field for measured and simulated data. Even though this function does not properly fit the tail of the profiles, the remaining of the curve is well represented. Moreover, the sigmoid fitting parameters have shown to be insensitive to simulation noise, as well as to the unfitted low dose region: variations of up to ± 20% on the dose values at the low dose points (i.e., points with less than 20% of maximum dose) resulted in less than 2% and 0.05% absolute fluctuation to the k and x_0 parameters, respectively. Hence, the sigmoid function, together with its fitting parameters, provide reliable information on the penumbra region. The same behavior is observed for inline profiles, for all fields analyzed and at both 15 mm and 100 mm depths in water. For all data sets, the adjusted R^2 are greater than 0.988 and the RMSEs are lower than 0.040.

$$D(x) = \frac{1}{1 + e^{-k(x-x_0)}} \tag{3}$$

The cost values are calculated as the percentage difference between the fitting parameters of the measured curve, k and x_0, and the fitting parameters k' and x_0' of the simulated curve, k_{cost} and x_{0cost} respectively (Eqs. (4) and (5)). These values offer more information than the χ^2, as the latter only provides an absolute value of disagreement, while k_{cost} and x_{0cost} provide information on the position and slope of the penumbra. The sign of k_{cost} indicates whether the simulated profiles have steeper or shallower slopes in the penumbra region, serving as a guidance for manipulation. To assess the overall improvement or worsening caused by the manipulations, each profile is fitted with two sigmoids: k_{cost} and x_{0cost} are calculated for both sides of the profile and the average of absolute values is considered.

$$k_{cost} = \frac{k - k'}{k}.\,100 \tag{4}$$

$$x_{0cost} = \frac{x_0 - x_0'}{x_0}.\,100 \tag{5}$$

Additional gamma (γ) evaluation [24] was performed for both PDD and lateral profiles using the (3%, 3 mm) criteria, as adopted by other authors for evaluation of the quality of simulated PDD and lateral profiles [17].

2.3. Cropping the PhSp

To reduce the simulation time and effectively increase its efficiency, a technique referred here as cropping has been introduced. In this

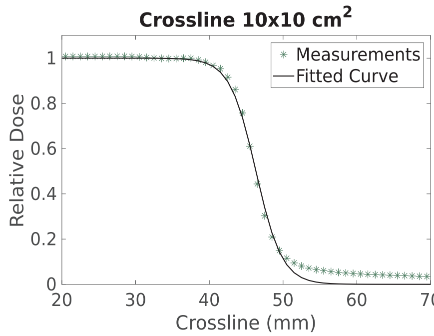

(a) Measurements

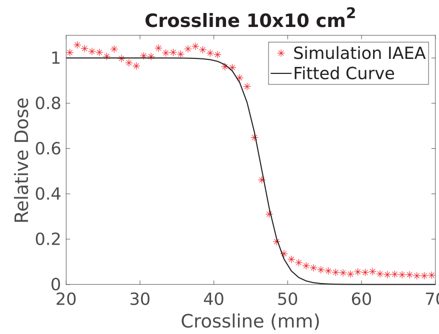

(b) Simulations (IAEA PhSp)

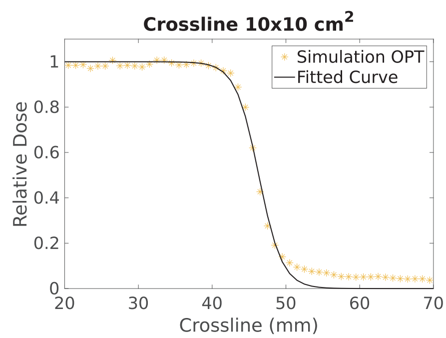

(c) Simulations (optimized PhSp)

Fig. 2. Crossline profiles fitted curves for the $10 \times 10\,\text{cm}^2$ field at 15 mm depth: for (a) Measurements, (b) Simulations performed with original PhSp and (c) Simulations performed with optimized PhSp. For all three data sets, the adjusted R^2 values are higher than 0.993; RMSE values are smaller than 0.038.

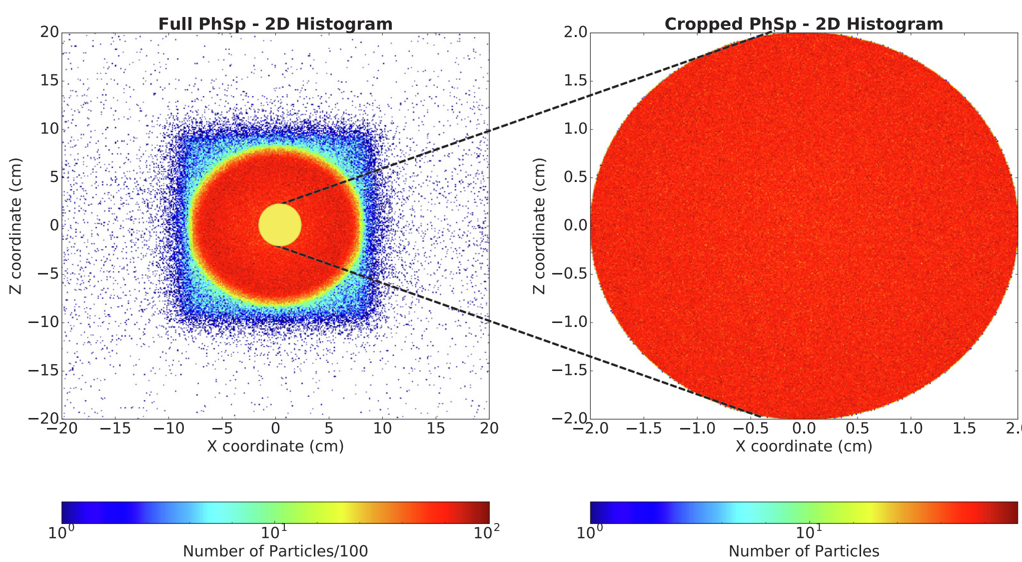

Fig. 3. Cropping: An example of cropping the original PhSp (left) to generate a cropped PhSp (right). In this example the cropping radius is 20 mm, which reduces the simulation time by a factor of 20.

technique a new PhSp is generated, cropping the original PhSp into a smaller radius as represented in Fig. 3. This radius has been referred to as the cropping radius. The position of the particles inside the PhSp, the dimension and spatial distribution of the scoring mesh and the field size determine the smallest appropriate cropping radius. To ensure that no relevant information is disregarded, the difference between simulated curves obtained with full and cropped PhSp should be under 3.0%. An example of cropping is presented in Fig. 3, in which the cropped PhSp only has the information of the particles within 0 to 20 mm.

PDD profiles from a $10 \times 10\,\text{cm}^2$ field were used for energy optimization. For PDD simulations, the column-like mesh was positioned in the center of the radiation field, and is therefore mostly, though not exclusively, dependent on dose deposited by the particles emerging from the center of the PhSp. To determine the acceptable cropping radius for PDD simulations, the PhSp was divided in radially symmetric regions, namely 0–5 mm, 5–10 mm, 10–15 mm, 15–20 mm, 20–40 mm and 40–60 mm. A large energy perturbation of 3 MeV was applied to the particles within each region individually, generating new PhSps, which were then used to simulate PDDs for a $10 \times 10\,\text{cm}^2$ field. The relevance of each region for the output was assessed by comparing the resultant PDD profiles to the one obtained using the original IAEA PhSp via the cost values. The lower the cost value, the lower the influence of the

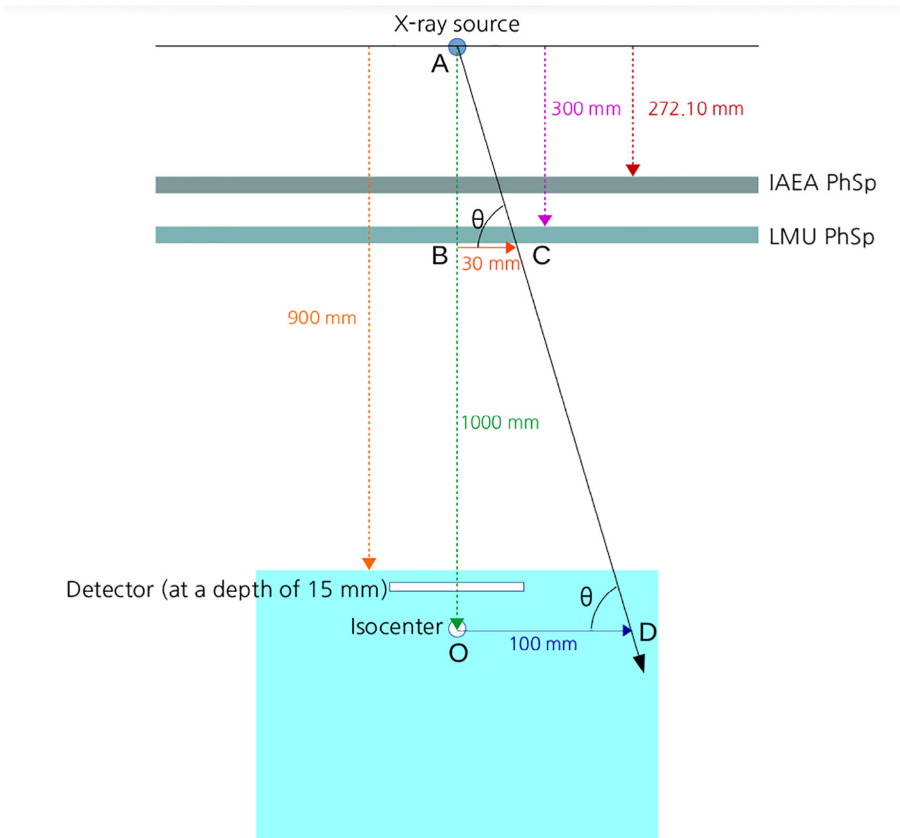

Fig. 4. Setup for lateral profile simulation: The isocenter is 1000 mm from the source (AO). The source-to-surface distance is 900 mm. The LMU PhSp is placed 300 mm from the source (AB). The 2D scoring mesh for lateral profiles (detector) is placed at 15 or 100 mm depth in the water phantom. (Not drawn to scale).

particles in the respective region to the PDD profile. The cropping radius was chosen as the one beyond which the perturbed region did not significantly influence the output of the simulation.

The effective cropping radii for lateral profiles simulations are determined based on geometric magnification (Fig. 4). The IAEA PhSp was generated on a plane placed 272.10 mm below the top of the Bremsstrahlung target (X-ray source). The LMU PhSp was generated 27.9 mm below the IAEA PhSp, and thus positioned 300 mm away from the source. For a certain field size in the isocenter plane (OD), the aperture of the collimator (BC), beyond which the radiation is blocked, can be calculated by Eq. (6). The distance from the source to the isocenter AO is 1000 mm, while AB is the distance from the target to the LMU PhSp.

$$BC = OD.\frac{AB}{AO} = OD.\frac{300\text{ mm}}{1000\text{ mm}} \tag{6}$$

This marks the radius of the LMU PhSp within which the particles are highly relevant for lateral profiles simulations, for an $OD \times OD$ cm^2 field, yielding a close approximation of the minimum cropping radius. The relevance of the particles beyond this region drops substantially, however the effective cropping radius was taken as at least twice the minimum cropping radius, as a conservative measure.

2.4. Optimization of energy

The optimization of energy was performed as an increase or decrease of the energies of the particles recorded in the original LMU PhSp. A perturbation of 0.2 MeV to the PhSp means that 0.2 MeV is added to the energy of every particle in the original PhSp, as presented in Fig. 5. This manipulation shifts the mean and median of the energy spectrum by the same amount. The only constraint identified was the annihilation peak at approximately 0.511 MeV, which should not be

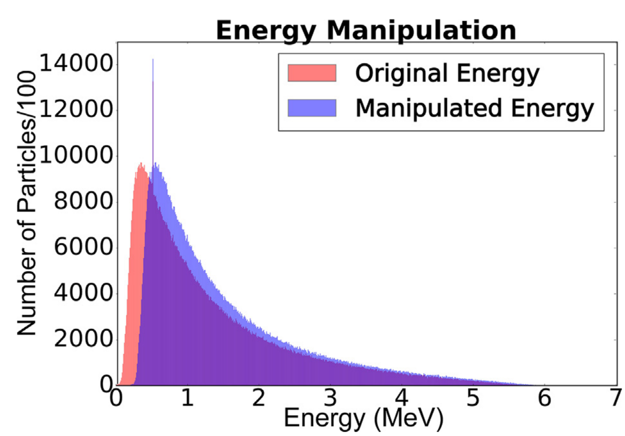

Fig. 5. Energy manipulation: Energy spectra of the PhSp with original energies (green) and perturbed energies (red). An increase of 0.2 MeV was applied to the original PhSp, meaning the energy of all particles, except the annihilation photons, were increased by 0.2 MeV. (For interpretation of the references to colour in this figure legend, the reader is referred to the web version of this article.)

affected. In this study only positive perturbations were considered. In PDDs previously simulated using the Elekta Precise IAEA PhSp, lower dose values were obtained than the dose values in the respective measured PDD, in the region of Transient Charged Particle Equilibrium, suggesting that the electron source used to generate the IAEA PhSp (5.75 MeV [16]) was of lower energy than the electron beam of the linac used for measurements. Moreover, higher energy values have been reported for the electron beam source when modeling the Elekta Synergy®linac [19,25].

To find the optimal perturbation factor for the energy, several PDD curves needed to be simulated using different PhSps with different energy perturbation factors. To optimize this process cropped PhSps, with a cropping radius of 20 mm, were used to simulate PDDs for a 10×10 cm^2 field.

New cropped PhSps with energy perturbations of 0.1, 0.2, 0.3 and 0.4 MeV were produced and used for PDD simulations. The cost values obtained for each simulation were analyzed and a local minimum between the curves simulated with PhSp perturbed with 0.3 and 0.4 MeV was identified. New PhSps with energy perturbations of 0.32, 0.34, 0.36 and 0.38 MeV were produced and PDDs were simulated. Once an optimal perturbation factor was found, it was applied to the full LMU PhSp and PDD curves for all fields were simulated in order to validate the manipulation. Lateral profiles in both inline and crossline directions, at 15 mm depth, were also simulated using the full PhSp with optimized energy.

2.5. Optimization of direction

The angular distribution of the particles emerging from the PhSp can be described in terms of their direction cosines P_x, P_y and P_z, which can be extracted from the LMU PhSp. Hereon they will be referred to as particle's direction for conciseness. The direction optimization was performed while respecting identified mathematical constraints. The divergence of the beam depends on the position of the particles, and increases for increasing distances from the center of the PhSp. The divergence can be defined by Eq. (7), where α is the angle between the particle's and the beam directions. In this study, the beam travels in the $-y$ direction, the x axis corresponds to the crossline direction (patient's left-right in the supine position) and the z axis corresponds to the inline direction (gun-target direction).

$$div = \tan\alpha = \sqrt{\frac{P_x^2 + P_z^2}{P_y^2}} \tag{7}$$

Any change in the direction of the particles emerging from the PhSp reflects as a change in the virtual photon source when traced back along the beam upstream, which is connected to the virtual electron focal spot. Experimental studies on the dependence of the dose lateral profiles and the electron focal spot have been presented [26,27].

2.5.1. The perturbation of P_x, P_y and P_z

For this manipulation, the energy-optimized PhSp was used as a starting point. Every particle in the PhSp has a divergence which is linearly dependent on its radial position, as can be seen from the green line in Fig. 6, described by Eq. (8). This linear relationship from hereon will be referred to as the beam divergence line. The individual divergences of the particles define the divergence of the photon beam macroscopically. Hence, by changing the divergence of every particle in a controlled manner, the macroscopic divergence of the entire beam can be steered. However, any changes must be consistent with the beam divergence line, i.e. the perturbed divergence must have a linear relationship with the radius as well. Thus, the only possible perturbation is to change the slope of the beam divergence line, as represented by the red line in Fig. 6, described by Eq. (9). To respect the low divergence of the particles in the center of the beam, the intersecting point c was kept unchanged. To manipulate the slope, the divergence of all the particles must be manipulated, hence P_x, P_y and P_z need to be perturbed. The equations and constraints to be considered for direction manipulation are listed from Eq. (8) to Eq. (13), where the variables with the circumflex (^) represent the manipulated quantities.

$$div(r) = mr + c, \tag{8}$$

$$\widehat{div}(r) = \hat{m}r + \hat{c}, \tag{9}$$

$$\hat{m} = \mu m, \tag{10}$$

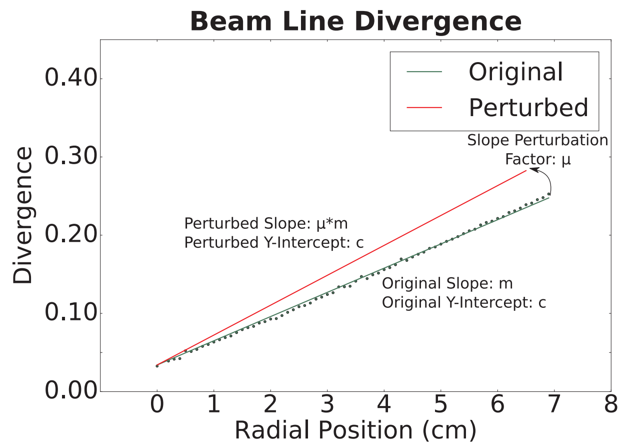

Fig. 6. Beam divergence line: The slope of the original beam divergence line (green), is perturbed by a factor μ, transforming it into the perturbed beam divergence line (red). The intercept value c remains unchanged. (For interpretation of the references to colour in this figure legend, the reader is referred to the web version of this article.)

$$\hat{c} = c, \tag{11}$$

$$\frac{\hat{P}_x}{\hat{P}_z} = \frac{P_x}{P_z} \tag{12}$$

$$P_x^2 + P_y^2 + P_z^2 = \hat{P}_x^2 + \hat{P}_y^2 + \hat{P}_z^2 = 1. \tag{13}$$

Eqs. (8) and (9) are the linear fitting functions for the original and the transformed divergence with respect to radius r, respectively. The transformation of the slope of the beam divergence line from m to $\hat{m}$, for a perturbation factor μ, is given by Eq. (10), while Eq. (11) keeps the divergence of the particles in the central region of the beam unaffected. Eq. (12) ensures that the beam does not curl around the central axis by maintaining the ratio between P_x and P_z. Eq. (13) is the normalization condition of the direction cosines which needs to be respected. Given a certain perturbation factor μ, the final transformations for P_x, P_y and P_z can be obtained using Eqs. (8)–(13) as summarized below.

$$\hat{P}_x^{\,2} = \frac{\omega^2}{\omega^2 + 1}\left(1 - \frac{1}{\gamma}\right), \tag{14}$$

$$\hat{P}_y^{\,2} = \frac{1}{\gamma}, \tag{15}$$

$$\hat{P}_z^{\,2} = \frac{1}{\omega^2 + 1}\left(1 - \frac{1}{\gamma}\right), \tag{16}$$

where

$$\omega = \frac{P_x}{P_z} \tag{17}$$

and

$$\gamma = \left(\mu\left(\sqrt{\frac{P_x^2 + P_z^2}{P_y^2}} - c\right) + c\right)^2 + 1. \tag{18}$$

2.5.2. Sigmoid fitting parameters versus μ

In order to identify possible correlations between the manipulation factor μ and its influence on simulated lateral profiles, 800 different perturbed PhSps were generated, with μ ranging from 0.001% ($\mu = 1.00001$) to 0.8% ($\mu = 1.008$) in 0.001% steps ($\Delta\mu = 0.00001$), and were then used to simulate lateral profiles. To optimize the process, this study was performed using the 2×2 cm^2 field and cropped PhSps with a cropping radius of 5 mm. Simulated profiles were fitted to sigmoid functions and the resultant fitting parameters were plotted against the

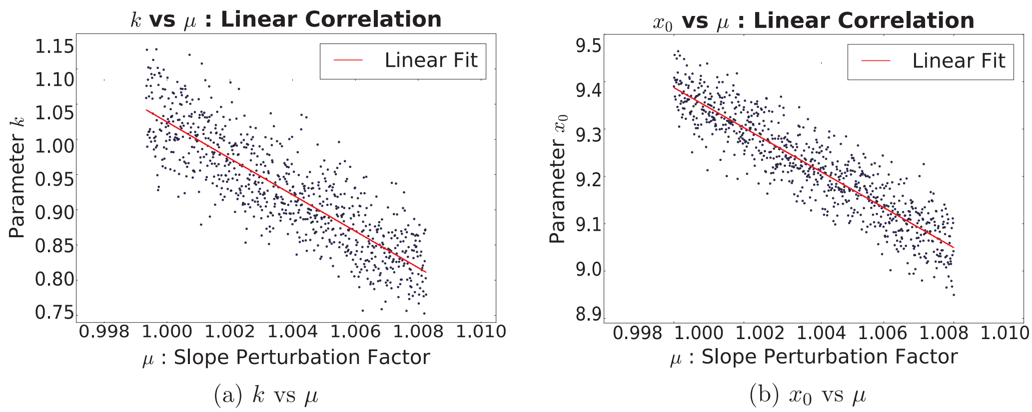

Fig. 7. Linear correlation between the manipulation factor μ and fitting parameters (a) k and (b) x_0.

different μ values (Fig. 7). Linear correlations between the perturbation factor and the two fitting parameters were identified.

It was observed that the sigmoid fitting parameters for multiple simulations with identical configuration were different, with differences up to 15% in few cases. This statistical uncertainty arises due to the finite number of particles stored inside a PhSp, especially when cropped PhSps are used. To account for this fluctuation, several simulations of the same configuration were performed and the medians of the fitting parameters were considered. The median is a more adequate quantity, as its value is less sensitive to the presence of outliers. An investigation was performed to determine the minimum number of identical simulations yielding stable median values. 50 identical simulations of lateral profiles were performed, for the $2 \times 2\,\text{cm}^2$ using cropped PhSp. The medians of k and x_0 were calculated using sets with different number of simulations, ranging from 1 to 50. It was observed that the median values become stable when 20 or more simulations are considered. From hereon in this study, 24 instances of simulations for the same configuration were performed, to ensure a stable result and a reasonable trade-off with the computational time.

2.5.3. *Finding the optimal* μ: μ_{op}

Thanks to the linear relationship between the sigmoid parameters and μ, the optimal perturbation factors for the particles' directions could be found following few simple steps, described below. The $10 \times 10\,\text{cm}^2$ field was used as the reference field in this investigation, with a cropping radius of 50 mm.

1. The energy-optimized PhSp was cropped to an effective cropping radius (Section 2.3).
2. A second cropped PhSp was generated and perturbed by a relatively large factor (0.8%) following Eqs. (14)–(16).
3. Lateral profiles were generated at 15 mm depth, using the two PhSps. 24 instances of simulation for each PhSp were performed.
4. All simulated profiles were fitted to sigmoids, and the medians of the resulting k and x_0 were calculated. A linear fit was applied to the two medians, with respect to μ (red line, Fig. 8).
5. The measured profile for the respective field size was fitted into a sigmoid curve and the parameters k and x_0 were extracted (green line in Fig. 8).
6. The intersections between the curves (green dots) represent the optimal perturbation factors obtained from k and x_0 (Fig. 8a and b respectively).
7. Steps (1–6) were repeated for 2×2, 5×5 and $20 \times 20\ \text{cm}^2$ fields and respective perturbation factors, specific to every field, were determined.
8. The resulting perturbation factors were calculated as the average of the individual factors from each field, considering the results obtained using the k parameter only.

Step 7 yields two optimal perturbation factors, based on k and x_0, which were one order of magnitude different from each other. However, the influence on the x_0 parameter due to changes in the divergence is much weaker than on k: a perturbation of 0.8% decreased the k by ~ 20%, while x_0 changed by ~ 0.75%. Perturbing the PhSp considering only the μ given by k increases the cost value of x_0, however the absolute difference was evaluated to be less than 0.3 mm (Fig. 8b). This behavior was observed for all fields analyzed. Hence, the perturbation factor obtained from k was given precedence over the perturbation factor from x_0, which will not be considered in the remaining sections of this study. It was ensured the final cost values for x_0 were within reasonable limits for all fields.

Moreover, the methodology described results in two different perturbation factors, one obtained when the inline profiles are considered (μ_{in}) and the other obtained based on crossline profiles (μ_{cr}). This essentially means that the divergence of the beam is not symmetric. For validation of each factor separately, the full energy-optimized PhSp was perturbed using the μ_{cr} determined by steps (1–8). Lateral profiles in the crossline directions were simulated 24 times for all fields considered, using the entire (full) PhSp. Fig. 8 shows the median values of k and x_0 for the $10 \times 10\,\text{cm}^2$, together with cost values obtained before (initial cost) and after (final cost) direction manipulation. The same was performed for μ_{in} with inline profiles.

The goal is to obtain one optimized PhSp that can be used for every simulation, therefore both factors need to be merged into one single factor, μ_{op}. As the cost values for the inline profiles were already low after the optimization of energy, focus was kept on optimizing the crossline profiles while maintaining the low cost values for inline.

Merging μ_{cr} *and* μ_{in} The methodology for merging both factors into one single factor μ_{op} is the result of several steps investigated throughout this work. It was initially assumed that the crossline profiles are largely dependent on the divergence of the particles near the crossline (x) axis, illustrated by the pink-shaded region in Fig. 9a. A similar assumption was made for the inline direction. These hypotheses can be described by Eq. (19), where the perturbation μ_ϕ is dependent on the angular position ϕ of the particles with respect to the crossline direction, with proportional contributions from μ_{cr} and μ_{in} (Fig. 9b).

$$\mu_\phi = cos(\phi)^2\mu_{cr} + sin(\phi)^2\mu_{in} \tag{19}$$

μ_ϕ ensures that the particles positioned exactly in the crossline and inline directions are perturbed by μ_{cr} and μ_{in}, respectively. However, particles positioned in the immediate surrounding might be perturbed insufficiently (for crossline) or excessively (for inline), affecting the quality of resultant profiles. To compensate for the fall-off of μ_ϕ, the values of μ_{cr} and μ_{in} were shifted to higher and lower values μ'_{cr} and μ'_{in}, respectively, according to Eqs. (20) and (21) (Fig. 9c, blue curve).

$$\mu'_{cr} = \zeta \cdot \mu_{cr}, \quad \zeta \geqslant 1 \tag{20}$$

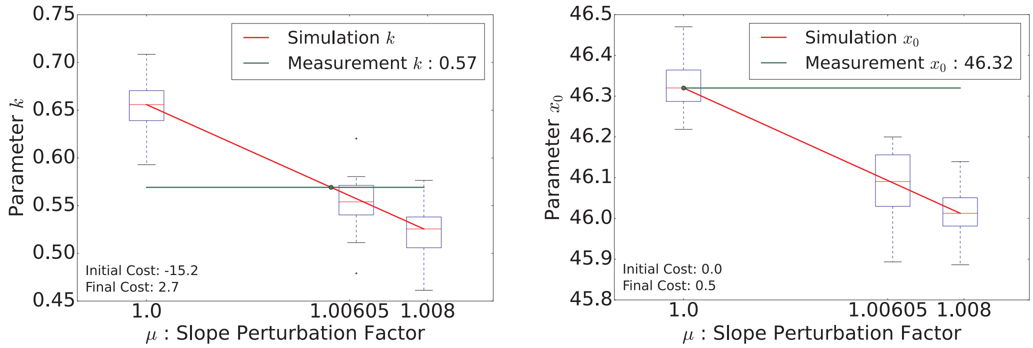

(a) k vs μ (b) x_0 vs μ

Fig. 8. Finding the optimal perturbation factor: from (a) k and (b) x_0. The green lines represent the fitting parameters of the measured crossline profile. The intersection of both green and red lines (green dot) gives the optimal perturbation factor in the crossline direction for the 10×10 cm^2 field. The optimized fitting parameters are represented by the boxplots in the middle. The final cost values are mentioned in the bottom of the plots.

$$\mu_{in}' = \eta \cdot \mu_{in}, \ \ \eta \leqslant 1 \tag{21}$$

Several combinations of μ_{cr}' and μ_{in}' were evaluated, with μ_{cr}' ranging from 1.00605 to 1.014 and μ_{in}' from 0.997 to 1.00051. A cross-correlation between μ_{cr} and inline profiles could be identified. The same was observed for μ_{in} and crossline profiles. This refutes the initial assumption of lateral profiles depending strictly on particles positioned locally. Furthermore, there is a trade-off between the quality of the simulated profiles in the inline and crossline directions. The cross-correlation, and subsequent trade-off, could be controlled by Eq. (22), a modification of Eq. (19), where the final optimization factor μ_{op} has a faster fall-off (Fig. 9c, pink curve).

$$\mu_{op} = cos(\phi)^6(\mu_{cr}' - 1) + sin(\phi)^6(\mu_{in}' - 1) + 1 \tag{22}$$

3. Results

3.1. Cropping the PhSp

Fig. 10 shows the comparison between PDDs simulated using the energy-perturbed PhSps (as described in 2.3) to simulations performed

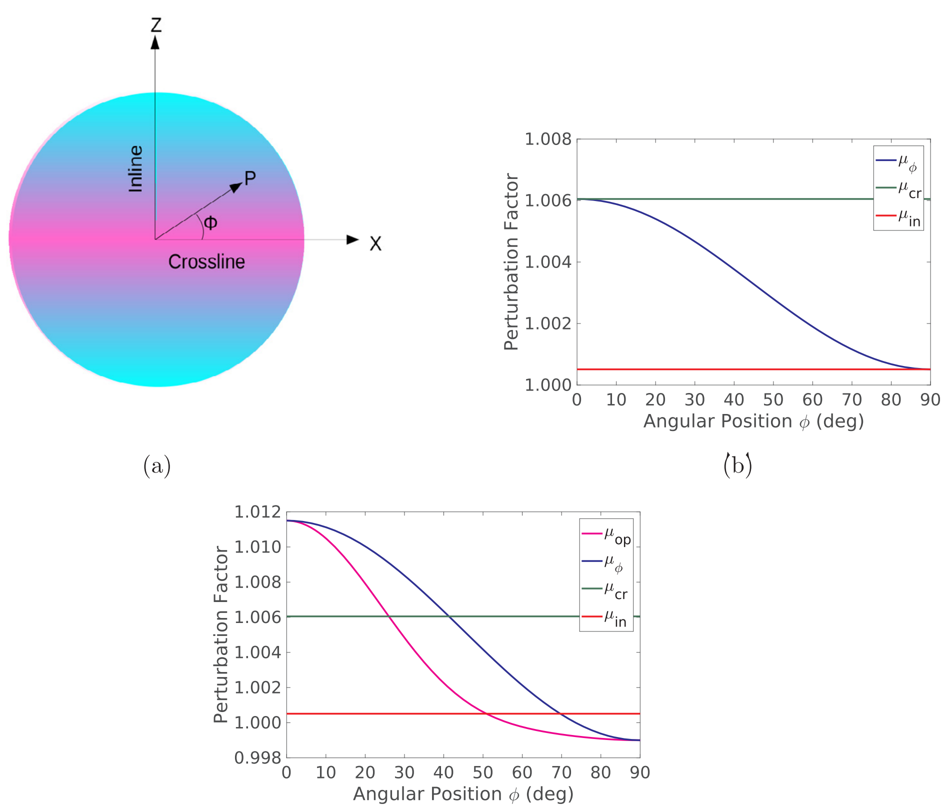

(a) (b) (c)

Fig. 9. Merging μ_{cr} and μ_{in}: (a) A schematic representation of the PhSp plane, where ϕ is the angular position of a particle with respect to the crossline direction. The pink shaded region represents the relevance of the particles for crossline dose profiles, as explained in the text (not shaded to scale); (b) The variation of μ_ϕ with ϕ; (c) μ_ϕ and μ_{op} for same μ_{cr}' and μ_{in}', a faster fall off can be observed for μ_{op}. The green and red lines are the individual perturbation factors, μ_{cr} and μ_{in} respectively. (For interpretation of the references to colour in this figure legend, the reader is referred to the web version of this article.)

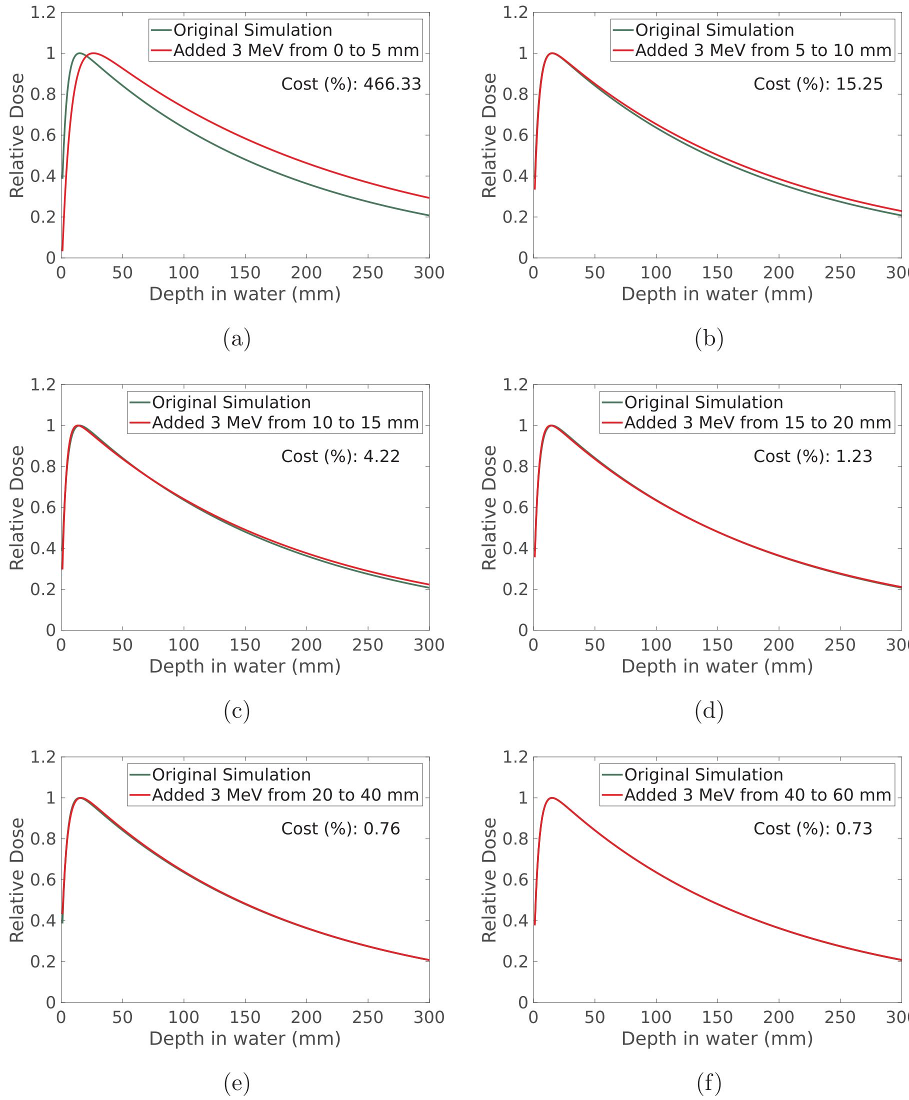

Fig. 10. PDD Cropping Radius: the effect of large energy perturbations to particles within different radial regions in the PhSp. The green curves represent the PDD profiles simulated using the original IAEA PhSp, while the red curves represent PDDs simulated using PhSps with 3 MeV energy perturbation to particles within a radial distance of (a) 0–5 mm, (b) 5–10 mm, (c) 10–15 mm, (d) 15–20 mm, (e) 20–40 mm and (f) 40–60 mm. It can be inferred that, beyond 20 mm, the particles' influence on the PDD profiles drops significantly.

using the original IAEA PhSp. For perturbation applied to regions beyond 20 mm (Fig. 10e and 10f), the cost values between both simulated curves are under 1.0%, indicating that the influence of particles positioned beyond this point on the PDD profiles drops significantly. Therefore, the cropping radius selected for PDD simulation was 20 mm.

Different cropping radii were used for simulating lateral profiles, depending on the field size (Table 1), as in Section 2.3. To ensure no relevant particles were disregarded, simulations performed using the cropped PhSp were compared to simulations performed with the full PhSp. The cropping radius was defined such that the cost between both simulations were under 3.0%, keeping a good trade-off with the simulation time.

Table 1
Cropping radii versus field sizes.

Field Size (cm^2)	Cropping Radius (mm)
2 × 2	20
5 × 5	20
10 × 10	30
20 × 20	50

The influence of the cropping radius on the determination of the perturbation factors μ_{cr} and μ_{in} was investigated, comparing two PhSps with cropping radii of 30 mm and 50 mm. For the 30 mm-cropped PhSp, μ_{cr} and μ_{in} were determined using only the 2 × 2, 5 × 5 and 10 × 10 cm^2 fields, as this cropping is too small for the 20 × 20 cm^2 field. All fields were used for the 50 mm-cropped PhSp. The absolute differences between the perturbation factors obtained with both cropped PhSps are under 0.01% for both μ_{cr} and μ_{in} (Table 2). Moreover, the simulation time was reduced by half when the smaller cropping radius was used. Therefore, a cropping radius of 30 mm, in combination with 3 field sizes, was sufficient for determining the individual perturbation factors.

Table 2
Optimal perturbation factors for crossline and inline directions, determined using PhSps with different cropping radii. The percentage differences are also presented.

Cropping Radius (mm)	μ_{cr}	μ_{in}
30	1.00601	1.00042
50	1.00605	1.00051
Difference (%)	0.004	0.009

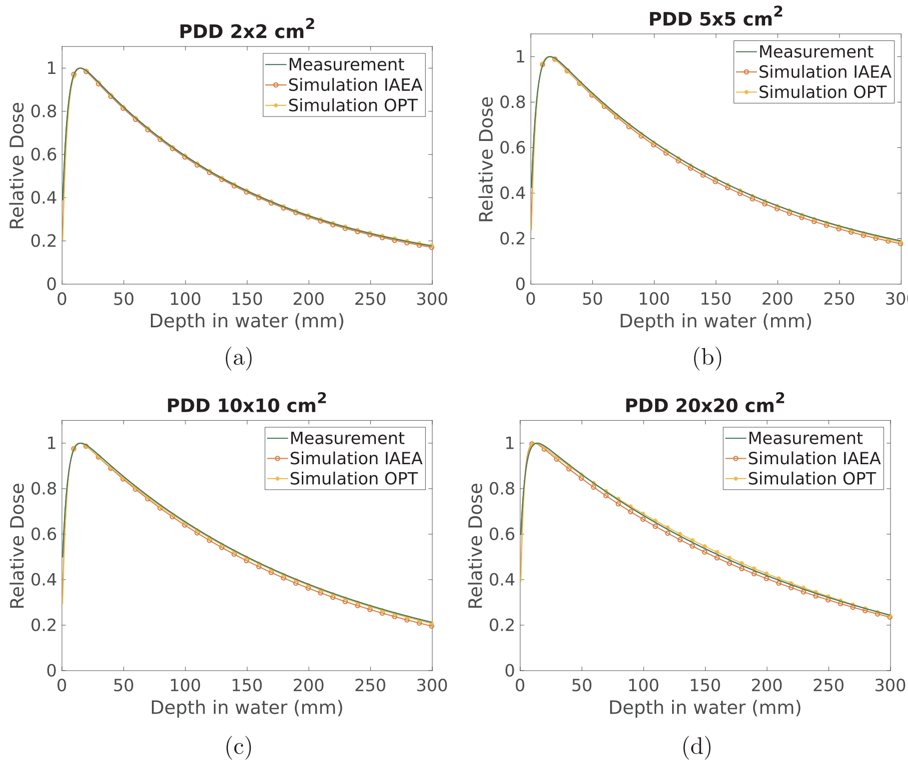

Fig. 11. PDD Comparison: Measured PDDs (green) compared to simulated PDDs using the original IAEA PhSp (red) and the energy-optimized PhSp (orange), for field sizes of (a) 2 × 2, (b) 5 × 5, (c) 10 × 10 and (d) 20 × 20 cm^2. All profiles have been generated using full PhSp for validation. (For interpretation of the references to colour in this figure legend, the reader is referred to the web version of this article.)

It is hard to determine the exact gain on time efficiency due to the cropping technique. The simulation time depends on many factors, such as the profile type, the field sizes and the specifications of the machine used. In this study, the simulations were performed in a computer cluster comprising machines with different specifications. Moreover, the workload on these machines might affect their performance. In general, when compared to simulations performed with the full PhSp, the simulation time dropped at least 60% when using the PhSp with the largest cropping radius (50 mm for lateral profiles of 20 × 20 cm^2 field). For PhSp with a 20-mm cropping radius (lateral profiles of 2 × 2 and 5 × 5 cm^2 and all PDDs), the simulation ran up to 20 times faster.

3.2. Optimization of energy

The PhSp with 0.32 MeV perturbation yielded the lowest cost values for PDD profiles for all fields analyzed. Fig. 11 shows the comparison between simulations performed using the original IAEA PhSp (red) and the full energy-optimized LMU PhSp (orange) to the measured curve (green). Table 3 shows the cost values before and after energy optimization. The γ passing rates, i.e. the percentage of points passing the (3%, 3 mm) criteria, are presented in Table 4, for simulations performed with the original and energy-optimized PhSp.

The energy optimization also improved the cost values for lateral profiles in the inline direction. For the crossline direction, no relevant changes were observed for the smaller fields, while important improvements were obtained for 10 × 10 and 20 × 20 cm^2 fields (Table 5).

Table 3
Initial and final cost values of PDD profiles, for the optimization of energy, when using the original and energy-manipulated full PhSp, respectively.

Field Size (cm^2)	Initial Cost (%)	Final Cost (%)
2 × 2	2.9	1.1
5 × 5	6.4	1.4
10 × 10	11.2	1.1
20 × 20	9.1	1.3

Table 4
Initial and final γ passing rates for PDD profiles, for the optimization of energy, when using the original and energy-optimized full PhSp, respectively.

Field Size (cm^2)	Initial γ (%)	Final γ (%)
2 × 2	94	97
5 × 5	95	99
10 × 10	92	98
20 × 20	96	97

Table 5
Initial and final cost values of lateral profiles in the inline and crossline directions, for the optimization of energy, when using the original and energy-optimized full PhSp, respectively.

Field Size (cm^2)	Inline		Crossline	
	Initial Cost (%) (IAEA PhSp)	Final Cost (%) (Energy Opt.)	Initial Cost (%) (IAEA PhSp)	Final Cost (%) (Energy Opt.)
2 × 2	4.3	3.1	24.2	22.4
5 × 5	8.5	3.1	26.3	26.6
10 × 10	15.7	6.0	22.1	17.6
20 × 20	8.6	1.2	16.4	12.9

3.3. Optimization of direction

The values obtained for the individual optimal perturbation factors were $\mu_{cr} = 1.00605$ and $\mu_{in} = 1.00051$ (Table 2). These factors were merged into a single optimization factor μ_{op} defined by Eq. (22). The

Table 6
Initial and final cost values of lateral profiles in the inline and crossline directions, at 15 mm depth, when using the original IAEA and final-optimized LMU PhSp, respectively.

	Inline		Crossline	
Field Size (cm^2)	Initial Cost (%) (IAEA PhSp)	Final Cost (%) (Opt. PhSp)	Initial Cost (%) (IAEA PhSp)	Final Cost (%) (Opt. PhSp)
2 × 2	4.3	1.6	24.2	13.2
5 × 5	8.5	2.9	26.3	10.6
10 × 10	15.7	4.6	22.1	8.1
20 × 20	8.6	0.8	16.4	8.0

Table 7
Initial and final cost values of lateral profiles in the inline and crossline directions, at 100 mm depth, when using the original IAEA and final-optimized LMU PhSp, respectively.

	Inline		Crossline	
3 Field Size (cm^2)	Initial Cost (%) (IAEA PhSp)	Final Cost (%) (Opt. PhSp)	Initial Cost (%) (IAEA PhSp)	Final Cost (%) (Opt. PhSp)
2 × 2	6.3	4.0	27.5	12.5
5 × 5	6.5	2.9	25.1	6.8
10 × 10	3.2	4.7	11.6	0.8
20 × 20	7.0	1.8	6.1	5.8

Table 8
Initial and final γ passing rates for lateral profiles in the inline and crossline directions, at 15 mm depth, when using the original IAEA and final-optimized full PhSp, respectively.

	Inline		Crossline	
Field Size (cm^2)	Initial γ (%)	Final γ (%)	Initial γ (%)	Final γ (%)
2 × 2	100	97	100	100
5 × 5	96	99	97	97
10 × 10	90	99	84	90
20 × 20	90	94	88	96

final perturbation factor μ_{op}, using $\mu'_{cr} = 1.012$ and $\mu'_{in} = 1.000$, yielded the best compromise for crossline and inline cost values and was therefore defined as the optimal perturbation factor for manipulation of particles' direction. A final optimized PhSp was produced, by perturbing the full energy-optimized PhSp with the optimal factor μ_{op}. Lateral profiles were simulated for all field sizes, at 15 and 100 mm depths in water. Tables 6 and 7 show the cost values obtained using the original and the final optimized PhSp. The γ passing rates with (3%, 3 mm) criteria are presented in Table 8 for simulations performed with the original and final-optimized PhSp at 15 mm depth. No relevant improvement was observed for the γ evaluation of profiles at 100 mm: for all fields, the passing rates were above 94% for profiles simulated with both original IAEA and full-optimized PhSp.

For a qualitative assessment of the improvement due to the optimization, Figs. 12 and 13 show the profiles at 15 mm for crossline and inline directions, respectively. For profiles at 100 mm depth, the same behavior was observed. As the cost values for the lateral profiles were calculated as the median of the individual values from 24 instances, the curves displayed in the figures are the sigmoid curves produced using the median values of k and x_0. The curve representing the measured profile is also the fitted sigmoid, for consistency.

PDD profiles were simulated after the momentum optimization, using the final optimized PhSp, to ensure that the low cost values obtained after energy optimization were maintained. Fig. 14 shows that the cost value for the 10 × 10 cm^2 PDD before and after momentum optimization remained low. The same behavior was observed for all the fields considered.

4. Discussion

A PhSp is essentially an enormous matrix of interconnected numerical values, defining the physical properties of the particles it stores. The PhSp is characteristic to the linac MC model which generates it. In this study, an attempt was made to manipulate a PhSp from one linac model to optimize it for another model. The complete optimization involved manipulating particles' energy and angular distribution, through manipulation of their direction cosines.

The cropping technique introduced was powerful to fasten the estimation of optimal perturbation factors for both energy and direction. A cropping radius of 20 mm was sufficient for determining the optimal energy manipulation factor. For the direction optimization, the manipulation factors μ_{cr} and μ_{in} can be obtained using a 30 mm-cropped PhSp. Furthermore, it was observed that a cropping radius of 20 mm was acceptable for determining the cost values of the profiles for 2 × 2 cm^2 field but was insufficient for finding the optimal perturbation factors. An even smaller cropping radius of 5 mm was unacceptable in calculating absolute cost values for any field, however it was useful for quick tests and analysis, such as the investigation performed in Section 2.5.2.

The optimization of energy was a straightforward addition operation. In this study, 0.32 MeV should be added to the energy of all particles inside the original LMU PhSp (correspondent to the IAEA Elekta Precise PhSp), in order to improve the simulation results for the Elekta Synergy linac. It was ensured that the 0.511 MeV annihilation photons remained unchanged. This energy perturbation decreases the PDD cost values to a maximum of 1.4% for all field sizes. Moreover, after energy optimization the agreement between measured and simulated lateral profiles in the inline directions increased for all field sizes, while for the crossline direction only for the bigger fields.

The optimization of the angular distribution, however, was very demanding. A distinct linear relationship between the sigmoid fitting parameters of the lateral profiles and the slope of the beam divergence line was detected, providing a direction on how to manipulate the divergence of the particles. The technique to manipulate the directions can be defined in 8 steps, resulting in two optimal perturbation factors based on inline and crossline profiles. Merging those into one single perturbation factor was very challenging. It was observed that crossline and inline dose profiles do not strictly depend on the divergence of particles positioned locally, implying that an attempt at optimizing the crossline profiles affected the inline profiles considerably, as can be seen in Fig. 15 for some combinations of μ'_{cr} and μ'_{in}. The inline cost increases even when the divergence of particles within a local angular distance from the inline direction is not considerably perturbed. Several steps were investigated for the development of a merging technique, until the best trade-off between crossline's and inline's cost values was achieved.

With the final optimized PhSp, remarkable improvements were obtained for the inline simulated profiles, in comparison to simulations performed with original IAEA PhSp: the absolute cost values dropped to under 4.6% and 4.7% for all fields analyzed, with reduction factors of at least 2.7 and 1.6, for 15 mm and 100 mm depth respectively. A small increase was observed for the cost value of 10 × 10 cm^2 field at 100 mm, however its final cost (4.7%) was comparable to the final values of other fields. For the crossline profiles, all absolute costs dropped to under 10.6% and 6.8% for the 15 mm and 100 mm respectively, except for the 2 × 2 cm^2 field. For the smallest field size, the final cost values were 13.2% and 12.5%, for 15 mm and 100 mm respectively. Even though the final costs values were above the desirable range in this study (5.0%), they still represent around 50% improvement, in comparison to the original IAEA PhSp. Moreover, Fig. 12 shows the

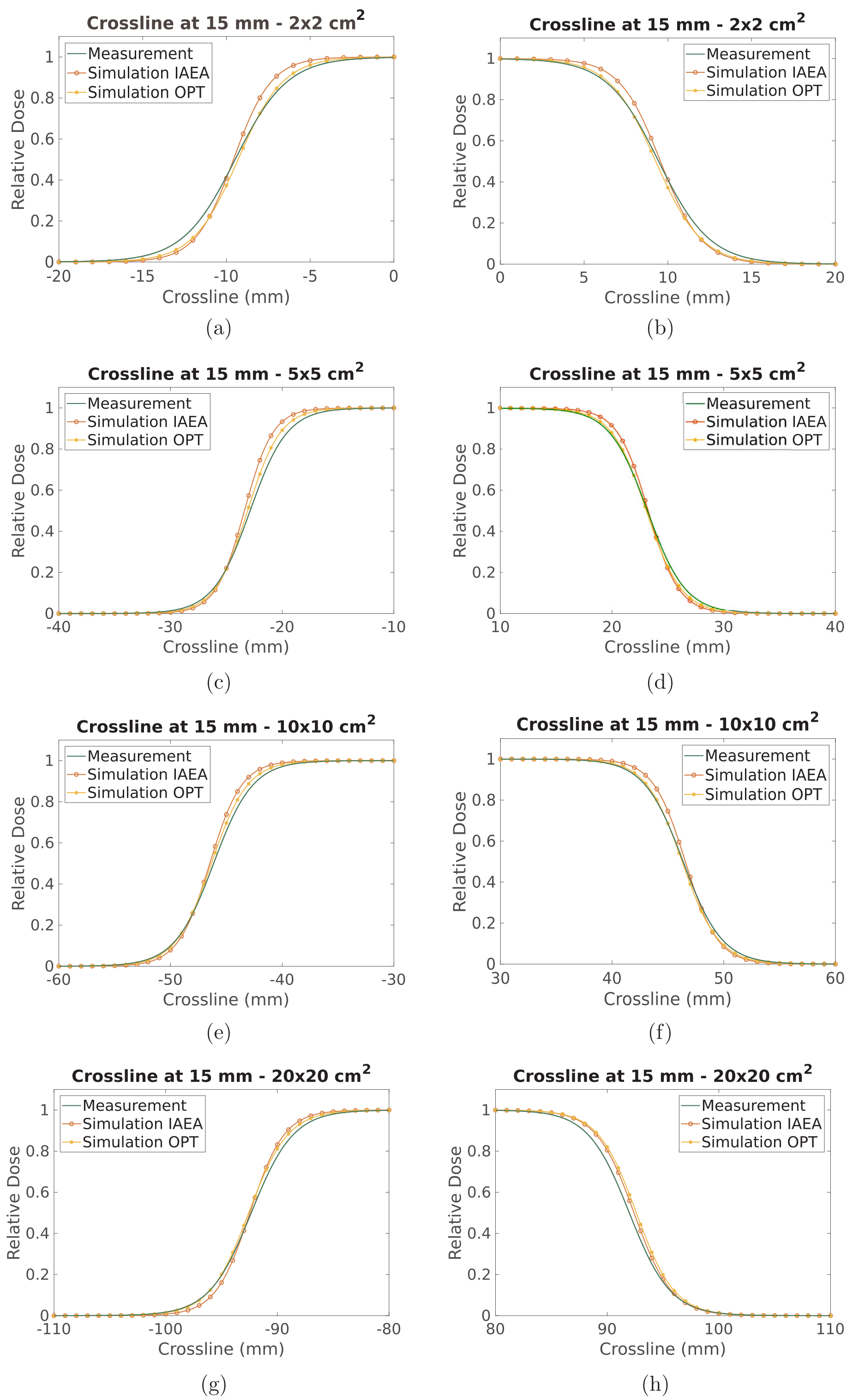

Fig. 12. Crossline Comparison at 15 mm depth: Measured crossline profiles (green) compared to the ones simulated using the original IAEA PhSp (red) and the final-optimized PhSp (orange), for field sizes of (a), (b) 2×2, (c), (d) 5×5, (e), (f) 10×10 and (g), (h) 20×20 cm^2. All profiles have been generated using full PhSp for validation. (For interpretation of the references to colour in this figure legend, the reader is referred to the web version of this article.)

qualitative improvement in the simulations.

The γ evaluation method was also used to assess the quality of the simulations and the improvements provided by the manipulations, however with the chosen criteria (3%, 3 mm) it failed in detecting small discrepancies between measured and simulated data, especially for the 2×2 cm^2 field. Aiming at improving the sensitivity, γ evaluation was performed with stricter distance-to-agreement (DTA) criteria (3%, 2 mm and 3%, 1 mm), but similar results were obtained. Stricter dose-difference (DD) criteria could not be used due to the magnitude of the simulation uncertainties (~3%). From these observations we can conclude that, in order to properly use the γ evaluation method for the PhSp optimization process, more stringent DD and DTA criteria are required, which can only be safely applied by reducing the statistical uncertainties of simulations (with related larger computational time).

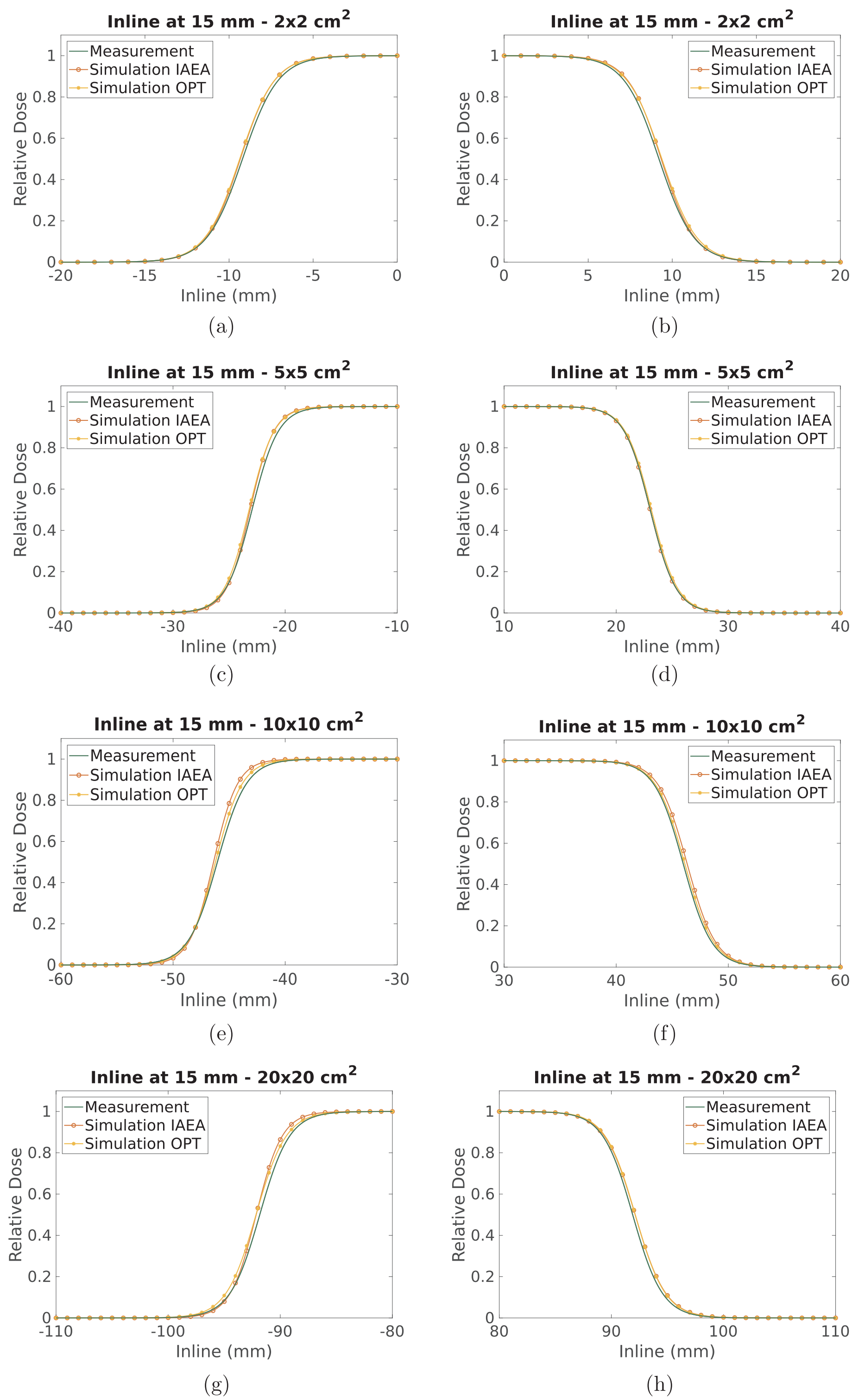

Fig. 13. Inline Comparison at 15 mm depth: Measured crossline profiles (green) compared to the ones simulated using the original IAEA PhSp (red) and the final-optimized PhSp (orange), for field sizes of (a), (b) 2 × 2, (c), (d) 5 × 5, (e), (f) 10 × 10 and (g), (h) 20 × 20 cm^2. All profiles have been generated using full PhSp for validation. (For interpretation of the references to colour in this figure legend, the reader is referred to the web version of this article.)

On the other hand, the introduced cost values can provide a valid alternative with less stringent statistical requirements. In particular, they offer very valuable information to the user, especially for the lateral profiles, as they provide insights into the nature of the discrepancies that can guide the user during the optimization process.

Furthermore, the goal of this work was to develop and test the feasibility of the methodology, which is an iterative process, meaning that the PhSp can be potentially further optimized. As a good compromise between results and simulation time, we decided to stop the iterations once all the costs dropped to under 50% of original values. For even better optimization, the search for the optimal manipulation factors can go through more steps:

1. In Section 2.5.3, steps 1 to 4 can be performed using more perturbed

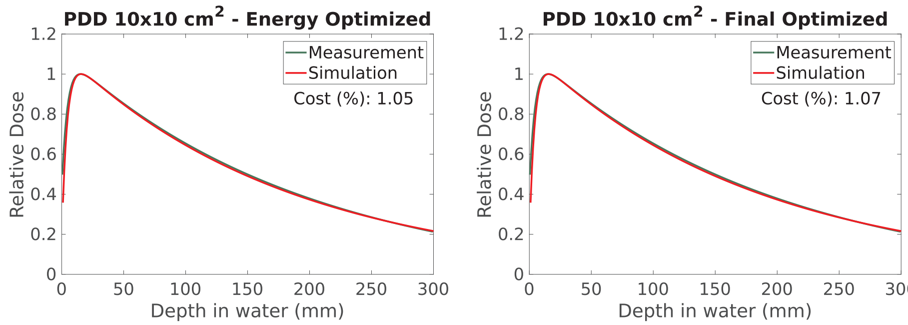

(a) (b)

Fig. 14. PDD profiles for the 10 × 10 cm^2 field before (a) and after (b) the optimization of direction: The low cost values obtained after energy optimization are maintained.

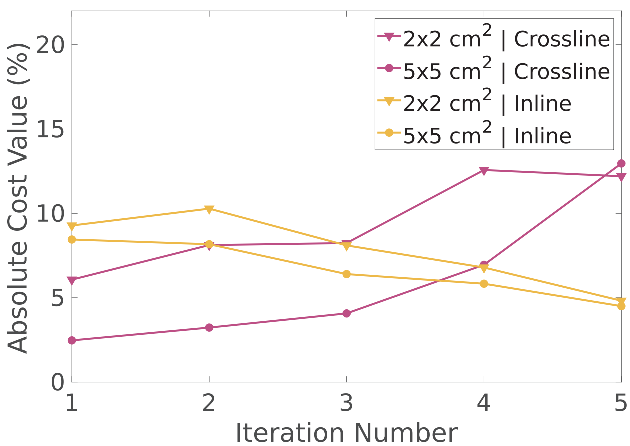

Fig. 15. Crossline and inline trade-off: Absolute cost behavior with multiple combinations of μ'_{cr} and μ'_{in}, represented by the horizontal axes (iteration number), for μ_ϕ. A trade-off between the crossline and the inline cost values is evident.

PhSps to obtain the linear fit (red curve, Fig. 8), which can potentially result in better values of μ_{cr} and μ_{in}.

2. An even more extensive investigation can be done, using a higher number of combinations of μ'_{cr} and μ'_{in} (Eqs. (20) and (21)).
3. Evaluation of lateral profiles in different directions (e.g. diagonal) could provide further information regarding the divergence of the beam.
4. Additional information can be obtained by evaluating different collimator angles (e.g. 90°).

It is also important to notice that, in general, a specific PhSp will not necessarily fit all machines of the same model: due to small differences in installations and settings, geometric parameters are essentially machine-specific, and so are the PhSps. The proposed methodology offers the user the flexibility to potentially optimize and tune a PhSp as much as desired.

Finally, the optimization of particles' energy and direction relates mostly to the electron source of the linac MC model used to generate the PhSp. Further differences in the geometries of the Elekta Precise and Synergy, which could greatly influence the output of the simulations [20], could not be assessed by this method and might justify possible limitations on the improvement that can be achieved.

5. Conclusions

Starting from the Elekta Precise IAEA PhSp, a final optimized PhSp to an Elekta Synergy®linac was obtained. Both the energy and direction of particles in the original PhSp were perturbed with respective optimal perturbation factors determined throughout this study. The cropping technique introduced was essential to this work. Remarkable improvements were obtained for the PDD and inline profiles simulations. For the crossline profiles the improvement in the cost values was less notable, however reduction of at least 50% was obtained. The PhSp could be potentially further optimized, as the method is an iterative process.

The present study proposes a general methodology for manipulation of an existing IAEA PhSp, generated and validated for a certain linac model, for the production of a new PhSp, which could be used for simulating a different linac. For the linac models considered in this work, valuable improvements were obtained in the simulated data with the resultant optimized PhSp. However even better agreement between measurements and simulations could be achieved by the full-linac-head simulation, if geometric details are available. The optimized PhSp should not replace the full modelling of the linac head, which should remain as the primary method of choice, however it offers an alternative for MC linac simulations when neither the geometric details, nor the validated IAEA PhSp files, are available for the user.

Acknowledgments

The authors thank Dr. Mark Podesta for the gamma-evaluation routine. This work was supported by the Brazilian National Council for Scientific and Technological Development (CNPq, Grant No. 201383/2015-2); the Saudi Ministry of Education; the Alexander von Humboldt Foundation; and the Munich-Centre for Advanced Photonics (MAP).

References

[1] Bielajew AF. History of Monte Carlo. In: Seco J, Verhaegen F, editors. Monte Carlo techniques in radiation therapy. Boca Raton: CRC Press; 2013. p. 3–16.
[2] Han T, Mikell J, Salehpour M, Mourtada F. MO-F-BRB-02: dosimetric comparison of acuros XB deterministic radiation transport method with Monte Carlo and model-based convolution methods in heterogeneous media. Med Phys 2011;38:3722.
[3] Fogliata A, Vanetti E, Albers D, Brink C, Clivio A, Knöös T, Nicolini G, Cozzi L. On the dosimetric behaviour of photon dose calculation algorithms in the presence of simple geometric heterogeneities: comparison with Monte Carlo calculations. Phys Med Biol 2007;52:1363–85.
[4] Sterpin E, Tomsej M, De Smedt B, Reynaert N, Vynckier S. Monte Carlo evaluation of the AAA treatment planning algorithm in a heterogeneous multilayer phantom and IMRT clinical treatments for an Elekta SL25 linear accelerator. Med Phys 2007;34:1665–77.
[5] Rogers DWO. Fifty years of Monte Carlo simulations for medical physics. Phys Med Biol 2006;51:R287–301.
[6] Verhaegen F, Seuntjens J. Monte Carlo modelling of external radiotherapy photon beams. Phys Med Biol 2003;48:R107.
[7] Almberg SS, Frengen J, Kylling A, Lindmo T. Monte Carlo linear accelerator simulation of megavoltage photon beams: independent determination of initial beam parameters. Med Phys 2012;39:40–7.
[8] Aljarrah K, Sharp GC, Neicu T, Jiang SB. Determination of the initial beam parameters in Monte Carlo linac simulation. Med Phys 2006;33:850–8.
[9] Belosi MF, Rodriguez M, Fogliata A, Cozzi L, Sempau J, Clivio A, Nicolini G, Vanetti E, Krauss H, Khamphan C, Fenoglietto P, Puxeu J, Fedele D, Mancosu P, Brualla L. Monte Carlo simulation of TrueBeam flattening-filter-free beams using Varian

phase-space files: comparison with experimental data. Med Phys 2014;41.
[10] Deng J, Jiang SB, Kapur A, Li J, Pawlicki T, Ma C-M. Photon beam characterization and modelling for Monte Carlo treatment planning. Phys Med Biol 2000;45:411–27.
[11] Cortés-Giraldo MA, Quesada JM, Gallardo MI, Capote R. An implementation to read and write IAEA phase-space files in GEANT4-based simulations. Int J Radiat Biol 2012;88:200–8.
[12] Kawrakow I, Walters BRB. Efficient photon beam dose calculations using DOSXYZnrc with BEAMnrc. Med Phys 2006;33:3046–56.
[13] Capote R, Jeraj R, Ma C, Rogers D, Sánchez-Doblado F, Sempau J, Seuntjens J, Siebers J. Phase-space database for external beam radiotherapy. Summary report of a consultants' meeting, Technical Report. International Atomic Energy Agency; 2006.
[14] Kawrakow I. Accurate condensed history Monte Carlo simulation of electron transport. I. EGSnrc, the new EGS4 version. Med Phys 2000;27:485–98.
[15] Salvat F, Fernández-Varea JM, Sempau J. Penelope-2008: a code system for monte carlo simulation of electron and photon transport. In: the Workshop Proceedings, June.
[16] Tonkopi E, McEwen MR, Walters BRB, Kawrakow I. Influence of ion chamber response on in-air profile measurements in megavoltage photon beams. Med Phys 2005;32:2918–27.
[17] Grevillot L, Frisson T, Maneval D, Zahra N, Badel JN, Sarrut D. Simulation of a 6 MV Elekta Precise Linac photon beam using GATE/GEANT4. Phys Med Biol 2011;56:903–18.
[18] Kairn T, Cassidy D, Sandford PM, Fielding AL. Radiotherapy treatment verification using radiological thickness measured with an amorphous silicon electronic portal imaging device: Monte Carlo simulation and experiment. Phys Med Biol 2008;53:3903–19.
[19] Francescon P, Cora S, Satariano N. Calculation of $k_{Qclin,Qmsr}^{fclin,fmsr}$ for several small detectors and for two linear accelerators using Monte Carlo simulations. Med Phys 2011;38:6513–27.
[20] Sheikh-Bagheri D, Rogers DWO. Sensitivity of megavoltage photon beam Monte Carlo simulations to electron beam and other parameters. Med Phys 2002;29:379–90.
[21] Podgorsak EB. External photon beams: physical aspects. In: Podgorsak EB, editor. Radiation oncology physics: a handbook for teachers and students. Vienna: International Atomic Energy Agency; 2006. p. 161–217.
[22] Podder TK, Bednarz G, Yu Y, Galvin JM. Physical characterization and comparison of two commercially available micro-MLCs. Phys Med 2011;27:52–7.
[23] Walters B, Kawrakow I, Rogers D. History by history statistical estimators in the BEAM code system. Med Phys 2002;29:2745–52.
[24] Low DA, Harms WB, Mutic S, Purdy JA. A technique for the quantitative evaluation of dose distributions. Med Phys 1998;25:656–61.
[25] Fleckenstein J, Jahnke L, Lohr F, Wenz F, Hesser J. Development of a Geant4 based Monte Carlo Algorithm to evaluate the MONACO VMAT treatment accuracy. Zeitschrift für Medizinische Physik 2013;23:33–45.
[26] Sterpin E, Chen Y, Lu W, Mackie TR, Olivera GH, Vynckier S. On the relationships between electron spot size, focal spot size, and virtual source position in monte carlo simulations. Med Phys 2011;38(3):1579–86.
[27] Wang LL, Leszczynski K. Estimation of the focal spot size and shape for a medical linear accelerator by monte carlo simulation. Med Phys 2007;34:485–8.